Supporting Information

Tetrazole-functionalized Cu-MOF for efficient C_2H_2/CO_2 separation

Jingjing Chen,[a] Fugang Li,[a] Zihao Zhao,[b] Xiaokang Wang,*[a] Rongming Wang,*[a] and Daofeng Sun*[a]

[a] Shandong Key Laboratory of Intelligent Energy Materials, School of Materials Science and Engineering, China University of Petroleum (East China), Qingdao Shandong 266580, China
[b] College of Chemistry and Chemical Engineering, China University of Petroleum (East China), Qingdao Shandong 266580, China

[*] *Corresponding author E-mail:* dfsun@upc.edu.cn; rmwang@upc.edu.cn; xiaokangwang0625@163.com

Table of Contents

Experimental Procedures **S2**
Materials and instruments **S2**
Synthesis of H_2BDC-tetrazole **S3**
Synthesis of UPC-115 ..... **S4**
Single-crystal X-ray diffraction **S5**
Gas sorption measurements **S6**
Breakthrough experiments **S7**
Computational methods **S8**
Figures S1-S16 ..... **S11**
Tables S1-S2 ..... **S19**
References **S21**

Experimental Procedures

Materials and instruments

All reagents were commercially available and used without further purification.

^{1}H nuclear magnetic resonance (NMR) spectrum was obtained on a Bruker 400 MHz nuclear magnetic resonance spectrometer. Single crystal X-ray diffraction experiment was carried out on a SuperNova diffractometer equipped with mirror Cu-Kα radiation (λ = 1.54184 Å) and an Eos CCD detector. Powder X-ray diffraction (PXRD) patterns were collected on a Bruker D8-Focus Bragg-Brentano X-ray powder diffractometer equipped with a Cu sealed tube at 40 kV and 15 mA. Data were recorded over a 2θ range of 5-50° with a step size of 0.02° and a scan speed of 5°/min. Thermogravimetric analysis (TGA) was performed on a Mettler Toledo TGA/DSC1 instrument under a static N_2 atmosphere with a heating rate of 10 °C/min at the range of 40-900 °C. Infrared (IR) spectroscopy spectrum was collected on a Nicolet 330 FTIR Spectrometer within 4000-400 cm^{-1} region. Gas sorption measurements were conducted on a Micrometritics ASAP 2020 surface area analyzer. Breakthrough experiments were carried out on BSD-MAB multi-component adsorption breakthrough curve analyzer monitored by Hiden HPR-20EGA mass spectrometer.

Synthesis of H_2BDC-tetrazole

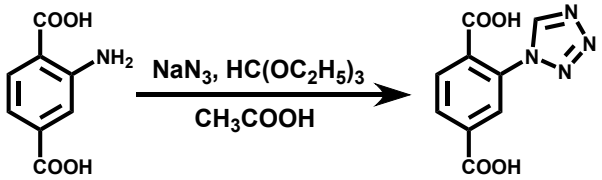

Scheme S1. Synthetic procedure of H_2BDC-tetrazole ligand

2-(1H-tetrazol-1-yl)terephthalic acid (H_2BDC-tetrazole) was synthesized according to our previous work.[1] To a suspension of 2-aminoterephthalic acid (18.1 g, 0.1 mol) and NaN_3 (7.8 g, 0.12 mol) in ethyl orthoformate (22 mL, 0.15 mol), glacial acetic acid (50 mL) was added while stirring, and the mixture was heated while stirring at 100 °C for 3 h. Then the reaction mixture was cooled, concentrated HCl (0.12 mol) was added, and the mixture was filtered and washed with water. The filtrate was evaporated under a vacuum, and the residue was extracted with hot ethanol. The solvent was removed, and the crude product was recrystallized from ethanol (50 mL). The precipitate that formed was separated by filtration, washed with water, and dried, affording a slightly gray solid (9.8 g, 42%). ^{1}H NMR (400 MHz, DMSO-d_6): δ = 8.16 (d, 2H), 8.26 (d, 1H), 9.88 (s, 1H), 13.72 (s, 2H).

Synthesis of UPC-115

A mixture of H_2BDC-tetrazole ligand (12.7 mg, 0.05 mmol), $Cu(NO_3)_2 \cdot 3H_2O$ (24.2 mg, 0.1 mmol), and 0.1 mL HBF_4 in 2 mL DMF and 0.5 mL H_2O was placed into a glass vial (10 mL) and heated at 80°C for 12 h. The vial was then cooled to room temperature at a rate of 5 °C/h. The obtained bright green block crystals (24.5 mg, 83% yield based on H_2BDC-tetrazole) were filtered, washed with methanol and dried in air.

Single-crystal X-ray diffraction

The as-synthesized crystals were taken from the mother liquid without further treatment, transferred to oil and mounted on to a loop for single crystal X-ray data collection. The data were collected on an Agilent Technologies SuperNova diffractometer equipped with graphite monochromatic Cu Kα radiation (λ = 1.54184 Å). With the help of Olex2, the structure was solved with the Superflip structure solution program using charge flipping and refined with the ShelXL refinement package using least squares minimization. The structure was treated anisotropically, whereas the hydrogen atoms were placed in calculated ideal positions and refined as riding on their respective nonhydrogen atoms. PLATON and SQUEEZE were used to calculate the diffraction contribution of the solvent molecules and thereby produced a set of partly solvent-free diffraction intensities.

Gas sorption measurements

The activated samples were prepared by immersing the as-synthesized MOFs in chromatography-grade methanol for solvent exchange followed by activation at 353 K under vacuum for 12 h. Gas adsorption experiments containing N_2 at 77 K, as well as C_2H_2, CO_2 and CH_4 at 273 and 298 K, were performed by using ASAP-2020 surface area analyzer. The Brunauer-Emmett-Teller (BET) specific surface area and the pore size distribution were calculated based on the N_2 adsorption isotherm at 77 K. Liquid nitrogen bath was used to stabilize the temperature at 77 K, respectively, whereas other test temperatures were maintained via a circulating water bath. The BET surface area was calculated using multi-point BET equation with the P/P_0 range of 0.005-0.035. Pore volume was calculated with the maximal adsorption capacity. Pore size distribution was calculated with the non-local density functional theory (NLDFT). The slight difference between the NLDFT pore size and the crystallographic channel dimensions reflects the dynamic nature of gas adsorption and the approximation inherent in the NLDFT model, but both values consistently confirm the microporous nature of UPC-115.

Breakthrough experiments

Breakthrough experiments were carried out on BSD-MAB multi-component adsorption breakthrough curve analyzer. The activated samples of UPC-115 (0.4678 g, packing length: 73 mm, packing density: 0.51 g/cm^3) were packed in a quartz tube (4 mm inner diameter × 210 mm length) and further flushed with He at 353 K for 10 h with a flow rate of 15 mL/min. System dead volumes before and after column are 7.0 and 3.7 mL, respectively, and the void volume is 3.0 mL. During the experiments at 298 K, the equimolar C_2H_2/CO_2 mixture was used at a flow rate of 2 mL/min, and the outlet gas was monitored by Hiden HPR-20EGA mass spectrometer. The flow rates of the gases were controlled by calibrated mass flow controllers (MFCs). The captured gas during the breakthrough experiment can be recovered by desorption process at 298 K with He at a flow rate of 10 mL/min.

Computational methods

Isosteric heat of adsorption

A Virial equation comprising the temperature-independent parameters a_i and b_j was employed to calculate the enthalpies of adsorption for C_2H_2 and CO_2, which were measured at 273 and 298 K.

$$\ln P = \ln N + \frac{1}{T}\sum_{i}^{m} a_i N_i + \sum_{j}^{n} b_j N_j$$

$$Q_{st} = -R\sum_{i=0}^{m} a_i N_i$$

Here, P is the pressure expressed in mmHg, N is the amount absorbed in mmol/g, T is the temperature in K, a_i and b_j are virial coefficients, and m, n represent the number of coefficients required to adequately describe the isotherms (herein, m =5 and n = 2). Q_{st} is the coverage-dependent isosteric heat of adsorption and R is the universal gas constant.

Selectivity based on ideal adsorbed solution theory

Before estimating the selectivity for binary gas mixture, the single-component gas adsorption isotherms were first fitted to dual-site Langmuir-Freundlich (DSLF) model:

$$q = q_{A,sat}\frac{b_A p^{n_1}}{1 + b_A p^{n_1}} + q_{B,sat}\frac{b_B p^{n_2}}{1 + b_B p^{n_2}}$$

where q is the amount of adsorbed gas (mmol/g), p is the bulk gas phase pressure (kPa), q_{sat} is the saturation amount (mmol/g), b is the Langmuir-Freundlich parameter (kPa^{-1}), and n is the Langmuir-Freundlich exponent (dimensionless) for two adsorption sites A and B indicating the presence of weak and strong adsorption sites. b_A and b_B are both temperature-dependent.

$$b_A = b_{A0}\exp\left(\frac{E_A}{RT}\right);\ b_B = b_{B0}\exp\left(\frac{E_B}{RT}\right)$$

The adsorption selectivity S_{ads} was calculated by ideal adsorbed solution theory:

$$S_{ads} = \frac{q_1/q_2}{p_1/p_2}$$

where q_1 and q_2 are the molar loadings in the adsorbed phase in equilibrium with the bulk gas phase, p_1 and p_2 are partial pressure.

Grand canonical Monte Carlo simulations

Grand canonical Monte Carlo (GCMC) simulations were carried out using the Sorption module of Materials Studio package. The Locate and Metropolis methods were used to predict the possible binding sites of C_2H_2 and CO_2 onto the framework. During the simulation, the C_2H_2 and CO_2 molecules including the frameworks were considered as rigid bodies. The optimal adsorption sites were simulated under 298 K and 100 kPa by the fixed loading task and Metropolis method. The atomic partial charges of the host MOF skeleton and all gas molecules were obtained from QEq method. The equilibration steps and the production steps were set to 5.0×10^6 and 1.0×10^7, respectively. The gas-skeleton interaction and the gas-gas interaction were characterized by the standard universal force field (UFF). The cut-off radius used for the Lennard-Jones interactions is 15.5 Å and the long-range electrostatic interactions were considered by the Ewald summation method.

In the present GCMC simulations, both the UPC-115 framework and the guest molecules were treated as rigid bodies. This approximation is common and computationally efficient, but it neglects potential framework flexibility (e.g., thermal motion or minor reorientation of tetrazole groups) that could slightly affect the absolute binding energies and density distributions. Nevertheless, the good agreement between the simulated preferential binding at tetrazole N sites and the experimental adsorption behavior supports the validity of the rigid model for identifying the primary adsorption mechanism.

Density functional theory calculations

Density functional theory (DFT) calculations were performed using Dmol3 module embedded in the Materials Studio software. Since it is a vast task to do the DFT calculations using a whole MOF unit cell, we used fragmented cluster models cleaved from unit cells representing the actual situations as high as possible, and the cleaved bonds at cluster boundaries were saturated by protons. The generalized gradient

approximation (GGA) with the Perdew–Burke–Ernzerhof (PBE) exchange-correlation functional was employed for the spin-unrestricted DFT calculations. The electronic wave functions were expanded by the double numerical plus polarization (DNP) basis set. The van der Waals correction was considered by Grimme to precisely describe the adsorption of gas molecules on the MOF framework. The convergence criterion was 1 × 10^{-5} Ha for energies, 2 × 10^{-3} Ha/ Å for forces, and 5 × 10^{-3} Å for atomic displacements. The global cutoff radius was set as 6.0 Å. In all the DFT calculations, all the atoms were allowed to fully relax. The adsorption energy (ΔE_{ads}) is expressed by the equation:

$$\Delta E_{ads} = E_{ads+fram} - E_{fram} - E_{ads}$$

where $E_{ads+fram}$, E_{fram}, and E_{ads} are the total energy of the adsorbate-framework adsorption system, adsorbent framework, and adsorbate molecule, respectively.

Equilibrium adsorption capacity and separation factor

The gas adsorption capacity can be calculated from the breakthrough curves by the equation:

$$q = \frac{F_i t_0 - \int_0^{t_0} F_e dt}{m V_m}$$

where q is the equilibrium adsorption capacity (mmol/g), F_i is the influent flow rate of the specific gas (mL/min), t_0 is the adsorption time (min), F_e is the effluent flow rate of the specific gas (mL/min), m is the mass of the adsorbents (g), and V_m is the molar volume of gas (L/mol).

The separation factor of the breakthrough experiment is determined as:

$$\alpha = \frac{q_1/q_2}{y_1/y_2}$$

where α is the separation factor, q is the equilibrium adsorption capacity, y is the molar fraction of gas.

Figures S1-S16

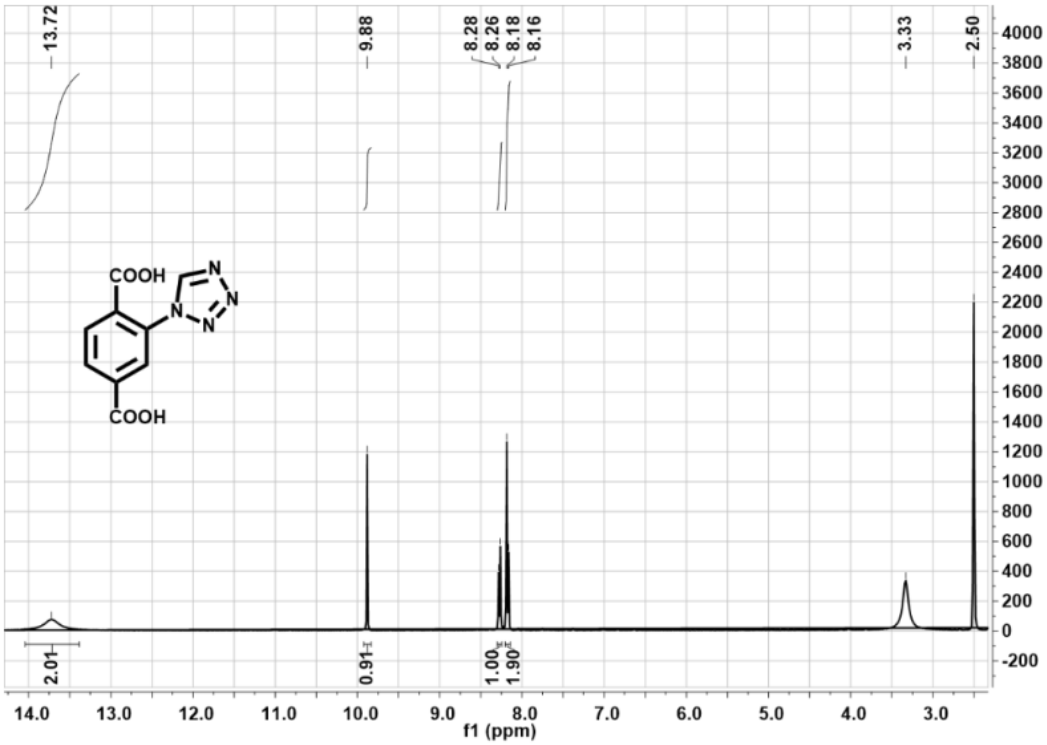

Fig. S1 ^{1}H NMR spectrum of H_2BDC-tetrazole.

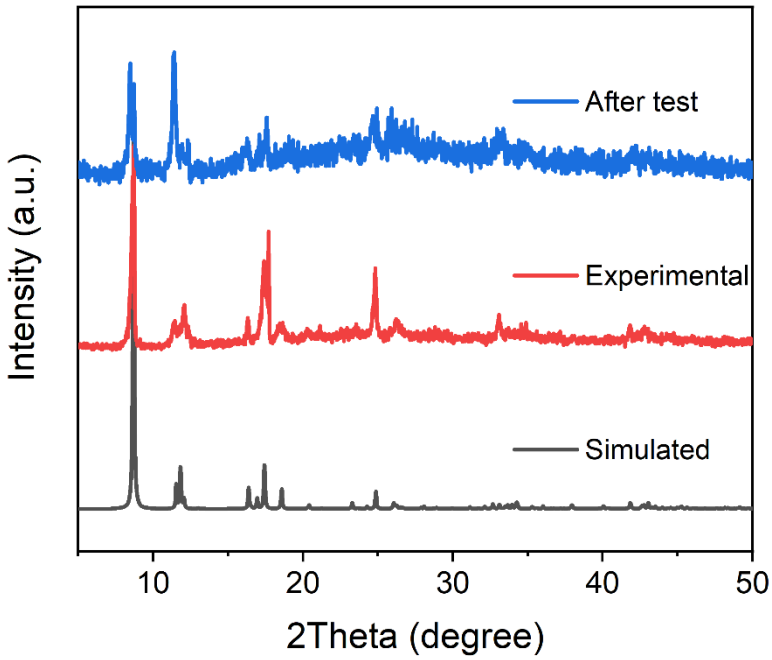

Fig. S2 PXRD patterns of UPC-115.

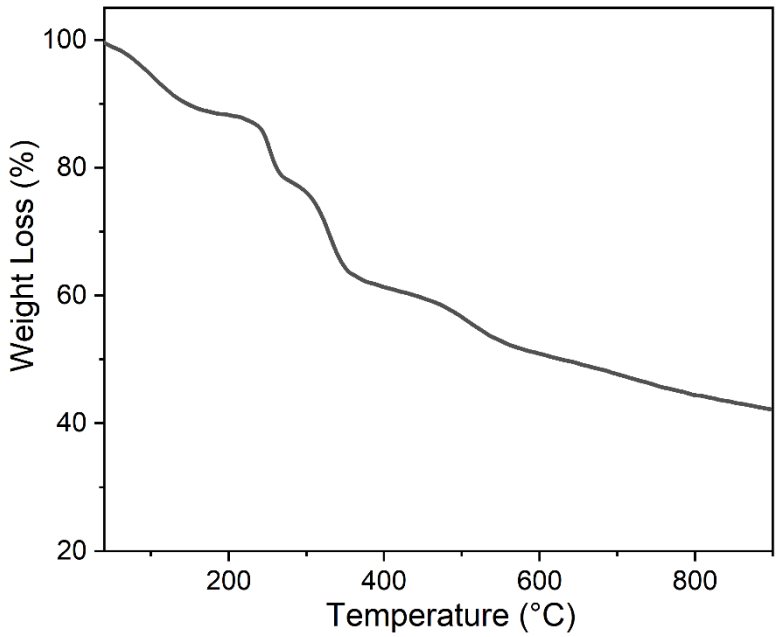

Fig. S3 TGA curve of UPC-115.

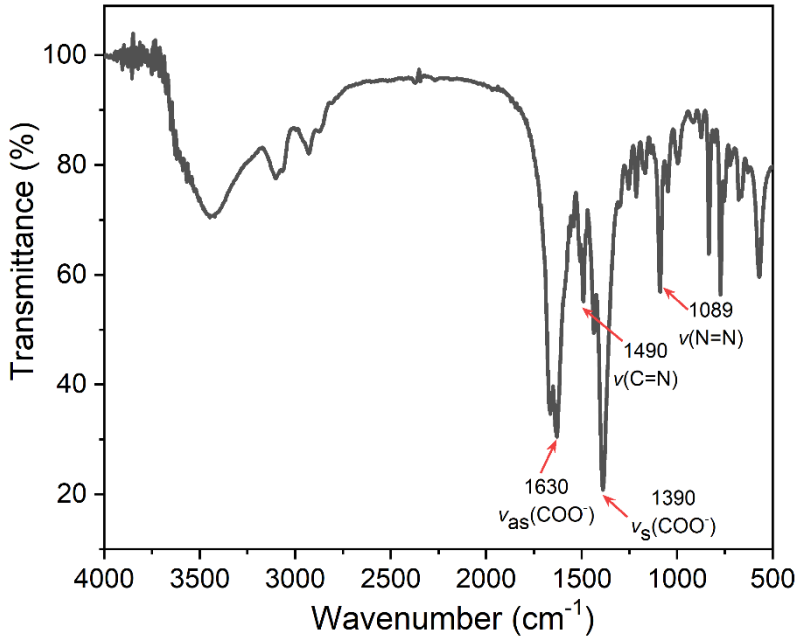

Fig. S4 IR spectrum of UPC-115.

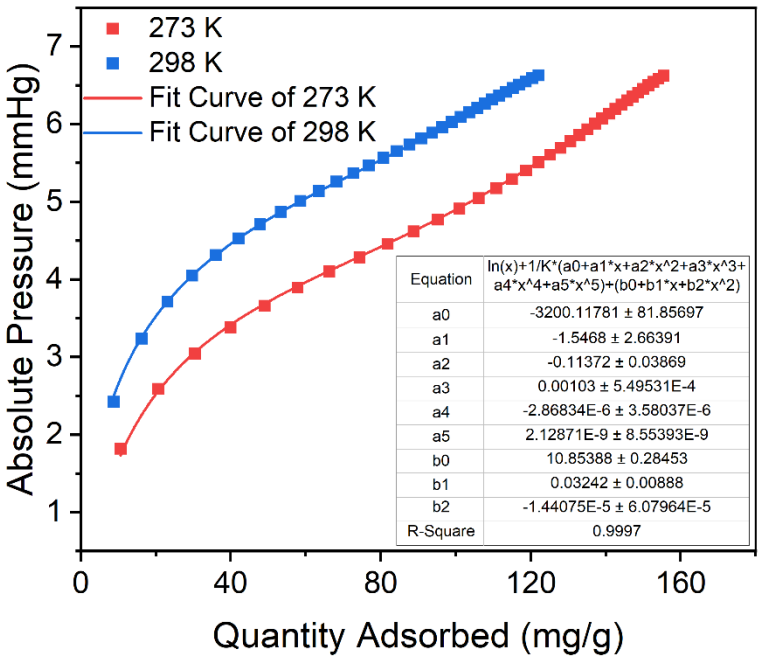

Fig. S5 Virial fitting of C_2H_2 for UPC-115.

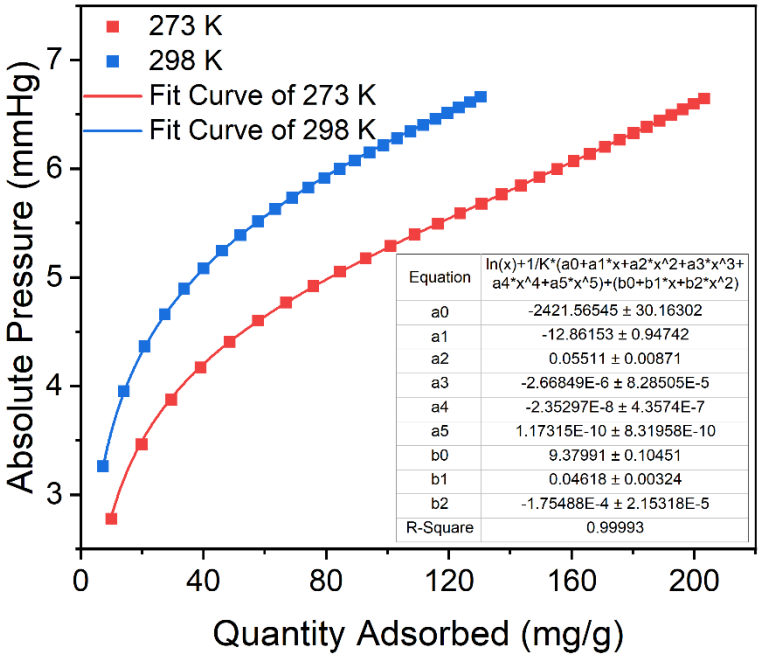

Fig. S6 Virial fitting of CO_2 for UPC-115.

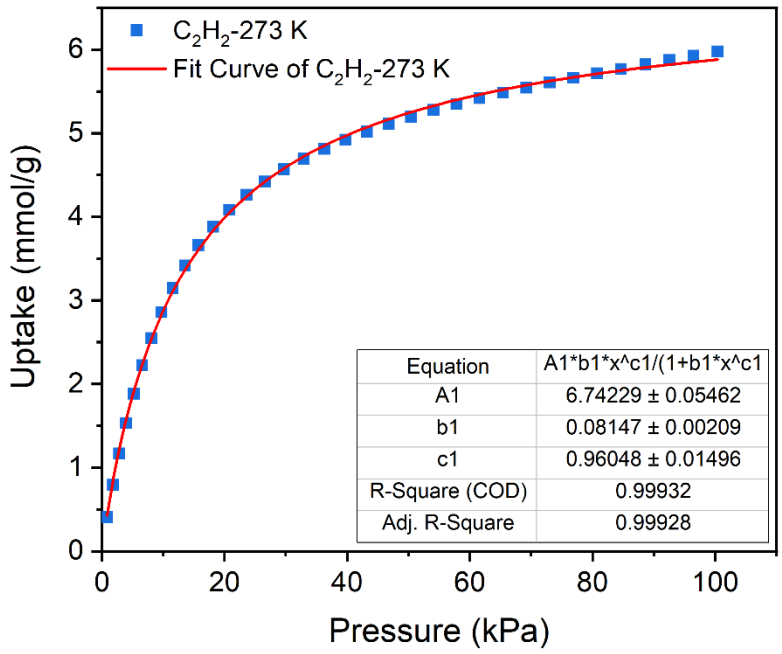

Fig. S7 Langmuir-Freundlich fitting of C_2H_2 for UPC-115 at 273 K.

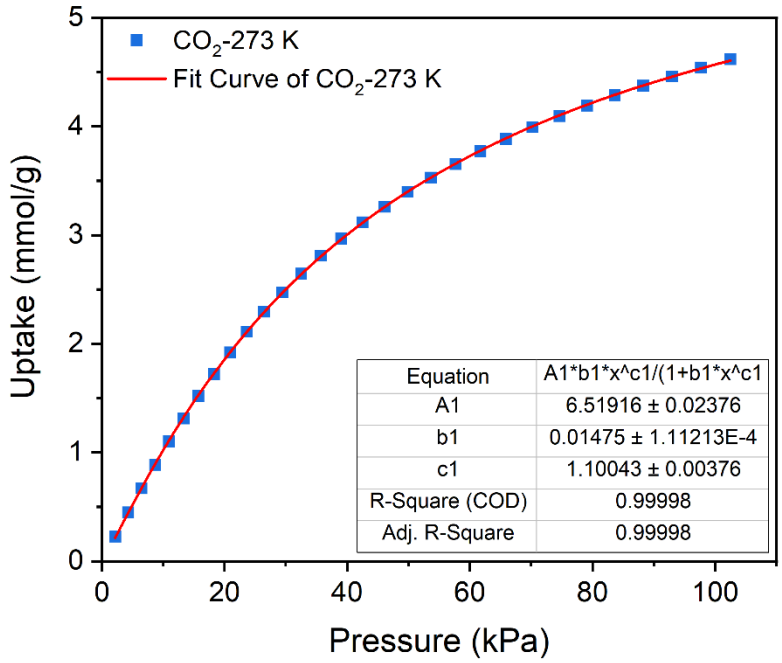

Fig. S8 Langmuir-Freundlich fitting of CO_2 for UPC-115 at 273 K.

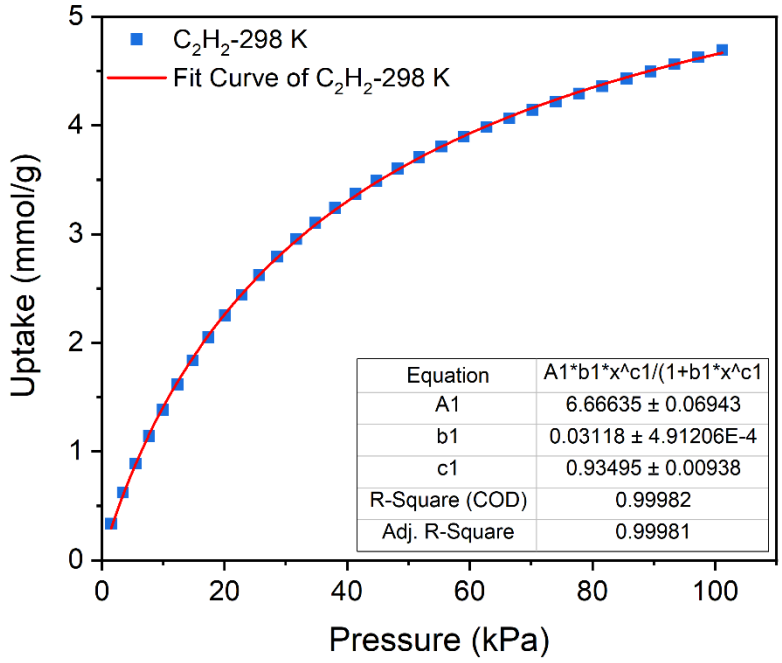

Fig. S9 Langmuir-Freundlich fitting of C_2H_2 for UPC-115 at 298 K.

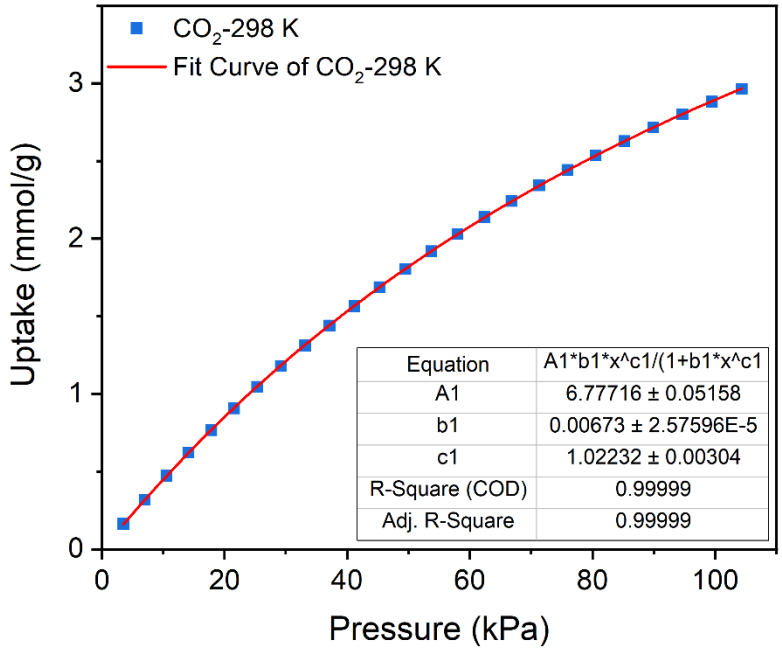

Fig. S10 Langmuir-Freundlich fitting of CO_2 for UPC-115 at 298 K.

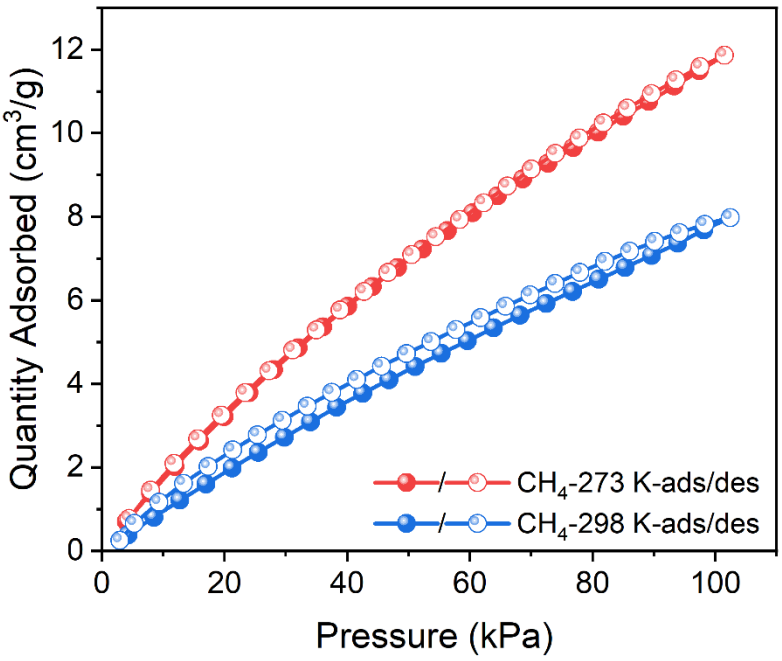

Fig. S11 Single-component adsorption/desorption isotherms of UPC-115 for CH_4 at 273 and 298 K.

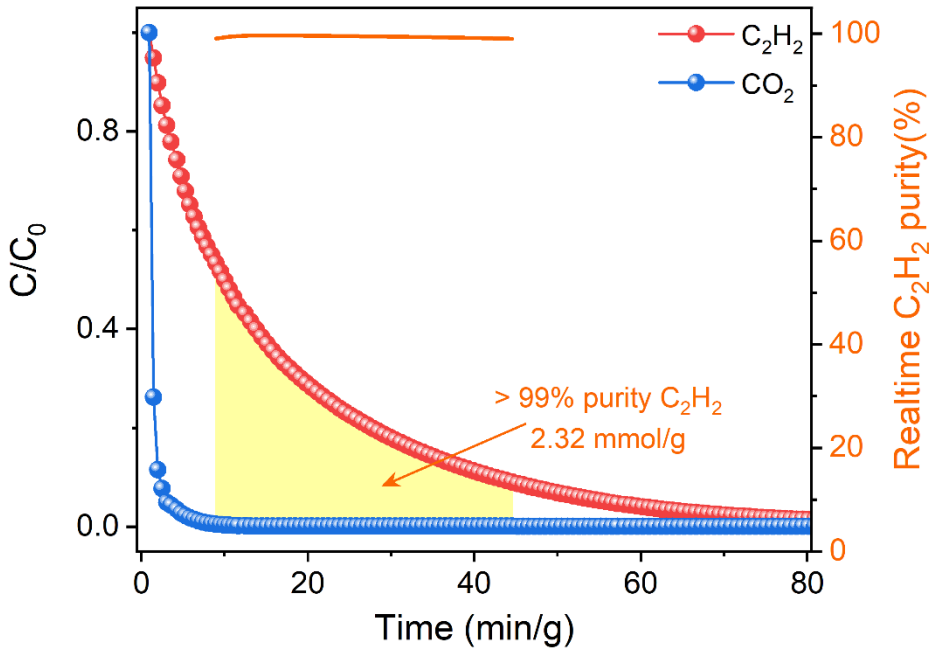

Fig. S12 Desorption curves of C_2H_2 and CO_2 from UPC-115-packed column collected by purging He with a flow rate of 10 mL/min at 298 K.

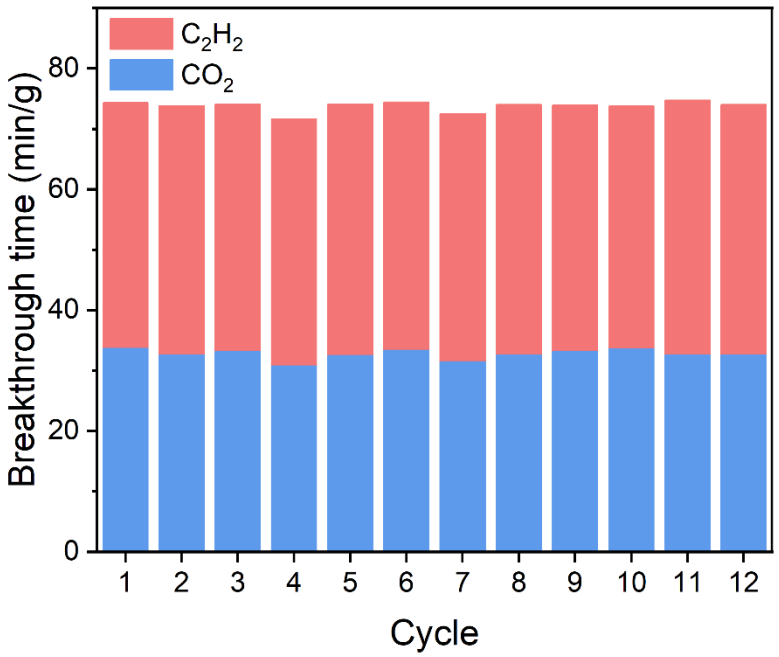

Fig. S13 Comparison of breakthrough time of C_2H_2 and CO_2 on UPC-115 over twelve consecutive cycles at 298 K and 1 bar.

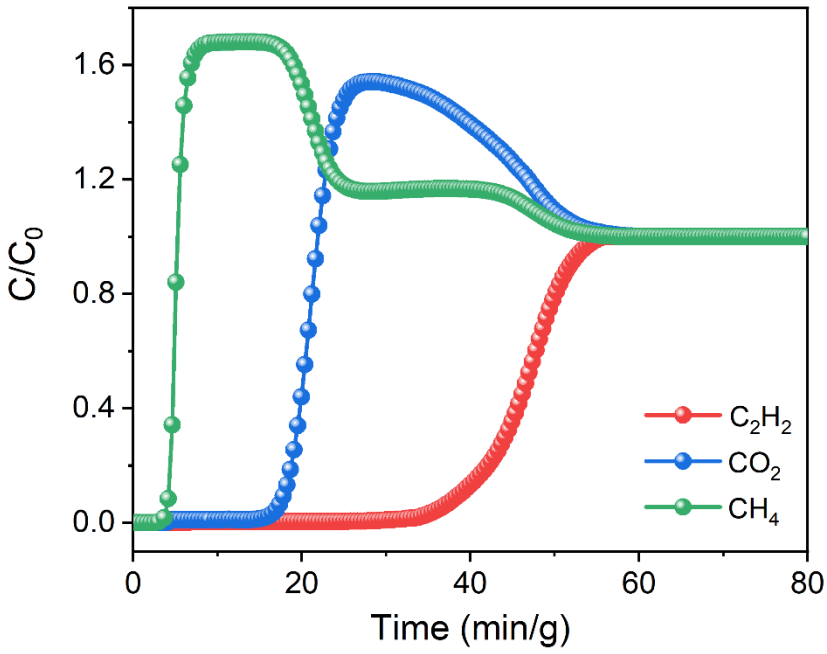

Fig. S14 Dynamic breakthrough curves of $C_2H_2/CO_2/CH_4$ (20/20/60, v/v/v) ternary mixture (5 mL/min) on UPC-115 at 298 K and 1 bar.

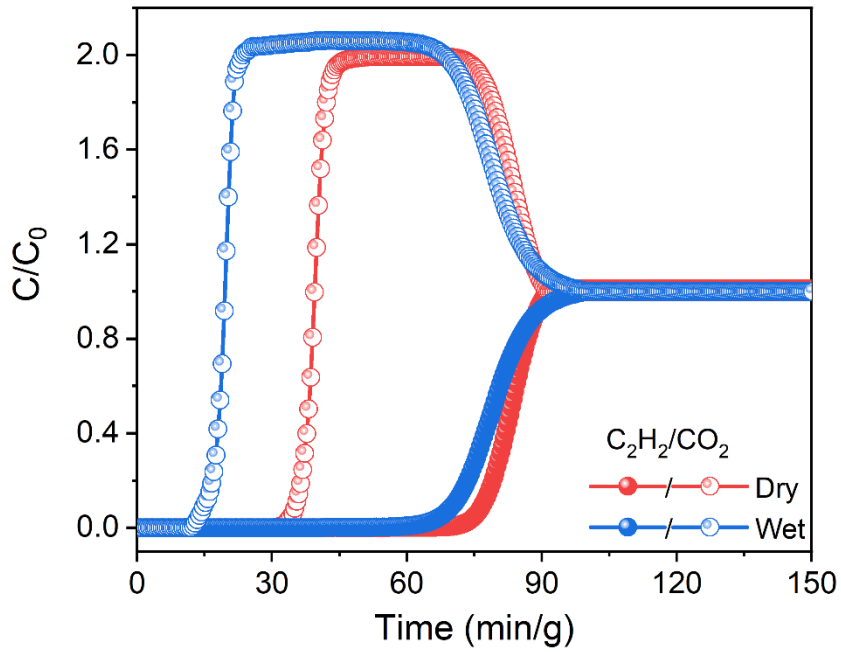

Fig. S15 Dynamic breakthrough curves of C_2H_2/CO_2 (50/50, v/v) mixture (2 mL/min) on UPC-115 under dry and humid condition (80% RH) at 298 K and 1 bar.

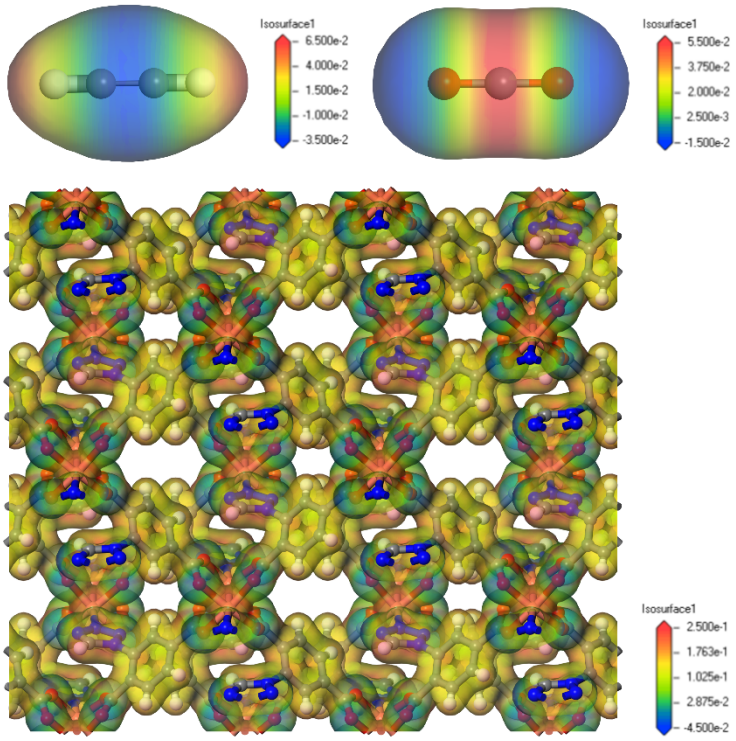

Fig. S16 Electrostatic potential map of C_2H_2, CO_2 and UPC-115.

Tables S1-S2

Table S1. Crystal data of UPC-115.

Compound	UPC-115
CCDC	2526912
Formula	$C_9H_4CuN_4O_4$
Formula weight	295.70
Temperature/K	150.01(10)
Crystal system	monoclinic
Space group	C2/c
a/Å	15.2696(8)
b/Å	15.3153(5)
c/Å	16.7734(11)
α/°	90
β/°	116.967(8)
γ/°	90
Volume/Å^3	3496.1(4)
Z	8
ρ g/cm^3	1.124
μ/mm^{-1}	1.257
F(000)	1176.0
2θ range for data collection	4 to 50.838
Index ranges	$-18 \le h \le 18$ $-18 \le k \le 18$ $-18 \le l \le 20$
Reflections collected	10383
R_{int}	0.0230
Data/restraints/parameters	3204/0/163
Goodness-of-fit on F^2	1.085
Final R indexes [I>=2σ (I)]	$R_1 = 0.0653$ $wR_2 = 0.1987$
Final R indexes [all data]	$R_1 = 0.0690$ $wR_2 = 0.2024$
Largest diff. peak/hole /eÅ^{-3}	0.87/-0.81

Table S2. Comparison of separation performance in MOFs at 298 K.

Materials	C_2H_2 uptake (cm^3/g)	C_2H_2 Q_{st} (kJ/mol)	IAST selectivity	Breakthrough interval time (min/g)	C_2H_2 productivity (mmol/g)	Ref.
BSF-1	52.6	31	3.3	–	–	[2]
CAU-10-H	89.8	27.4	4.0	45	–	[3]
CPL-1	45.0	45.5	11.7	~13	–	[4]
CPL-1-NH_2	41.2	50.0	118.9	27	–	[4]
FeNi-M'MOF	96.1	27	24	28.5	–	[5]
FJU-90a	180	25.1	4.3	–	–	[6]
JCM-1	75	36.9	13.7	–	–	[7]
JNU-1	–	13	3.6	34.1	–	[8]
Ni(4-DPDS)$_2$$CrO_4$	67.0	75.4	67.7	100	–	[9]
NKMOF-1-Ni	61.0	60.3	25	–	–	[10]
SNNU-45	134	39.9	4.5	79	–	[11]
TIFSIX-2-Cu-i	91.8	46.3	6.5	~93	–	[12]
UTSA-300a	68.9	57.6	743	12.8	–	[13]
UTSA-74a	108.2	31	9	–	–	[14]
ZJU-74	85.7	45	36.5	~33.6	3.01 (91%)	[15]
FJUT-1	133.2	43.75	4.06	31.7	2.12 (99.5%)	[16]
JXNU-5	55.9	32.9	–	10	–	[17]
M'MOF-2a	–	37.7	1.89	–	–	[18]
Ni(dpip)	83.6	41.7	2	–	–	[19]
SNNU-16	70.2	52.6	2.0	18	–	[20]
ZNU-1	76.3	54.0	56.6	–	2.4 (99.5%)	[21]
Cu^I@UiO-66-(COOH)$_2$	98.5	74.5	185.0	46.3	–	[22]
SOFOUR-TEPE-Zn	89.1	45.6	16833	59.1	2.68 (99.5%) 1.48 (99.99%)	[23]
Cu(bdc)	32.4	24.4	1.65	–	–	[24]
UPC-115	105.14	26.60	3.50	40.68	2.32 (99%)	This work

References

(1) Fan, W.; Peh, S. B.; Zhang, Z.; Yuan, H.; Yang, Z.; Wang, Y.; Chai, K.; Sun, D.; Zhao, D. Tetrazole-Functionalized Zirconium Metal-Organic Cages for Efficient C_2H_2/C_2H_4 and C_2H_2/CO_2 Separations. *Angew. Chem. Int. Ed.* **2021**, *60* (32), 17338–17343. DOI: 10.1002/anie.202102585.

(2) Zhang, Y.; Yang, L.; Wang, L.; Duttwyler, S.; Xing, H. A Microporous Metal-Organic Framework Supramolecularly Assembled from a Cu^{II} Dodecaborate Cluster Complex for Selective Gas Separation. *Angew. Chem. Int. Ed.* **2019**, *58* (24), 8145−8150. DOI: 10.1002/anie.201903600.

(3) Pei, J.; Wen, H. M.; Gu, X. W.; Qian, Q. L.; Yang, Y.; Cui, Y.; Li, B.; Chen, B.; Qian, G. Dense Packing of Acetylene in a Stable and Low-Cost Metal-Organic Framework for Efficient C_2H_2/CO_2 Separation. *Angew. Chem. Int. Ed.* **2021**, *60* (47), 25068−25074. DOI: 10.1002/anie.202110820.

(4) Yang, L.; Yan, L.; Wang, Y.; Liu, Z.; He, J.; Fu, Q.; Liu, D.; Gu, X.; Dai, P.; Li, L.; Zhao, X. Adsorption Site Selective Occupation Strategy within a Metal–Organic Framework for Highly Efficient Sieving Acetylene from Carbon Dioxide. *Angew. Chem. Int. Ed.* **2021**, *60* (9), 4570−4574. DOI: 10.1002/anie.202013965.

(5) Gao, J.; Qian, X.; Lin, R. B.; Krishna, R.; Wu, H.; Zhou, W.; Chen, B. Mixed Metal–Organic Framework with Multiple Binding Sites for Efficient C_2H_2/CO_2 Separation. *Angew. Chem. Int. Ed.* **2020**, *59* (11), 4396−4400. DOI: 10.1002/anie.202000323.

(6) Ye, Y.; Ma, Z.; Lin, R.-B.; Krishna, R.; Zhou, W.; Lin, Q.; Zhang, Z.; Xiang, S.; Chen, B. Pore Space Partition within a Metal–Organic Framework for Highly Efficient C_2H_2/CO_2 Separation. *J. Am. Chem. Soc.* **2019**, *141* (9), 4130−4136. DOI: 10.1021/jacs.9b00232.

(7) Lee, J.; Chuah, C. Y.; Kim, J.; Kim, Y.; Ko, N.; Seo, Y.; Kim, K.; Bae, T. H.; Lee, E. Separation of Acetylene from Carbon Dioxide and Ethylene by a Water-Stable Microporous Metal–Organic Framework with Aligned Imidazolium Groups inside the Channels. *Angew. Chem. Int. Ed.* **2018**, *57* (26), 7869−7873. DOI: 10.1002/anie.201804442.

(8) Zeng, H.; Xie, M.; Huang, Y. L.; Zhao, Y.; Xie, X. J.; Bai, J. P.; Wan, M. Y.; Krishna, R.; Lu, W.; Li, D. Induced Fit of C_2H_2 in a Flexible MOF Through Cooperative Action of Open Metal Sites. *Angew. Chem. Int. Ed.* **2019**, *58* (25), 8515−8519. DOI: 10.1002/anie.201904160.

(9) Zheng, F.; Chen, R.; Ding, Z.; Liu, Y.; Zhang, Z.; Yang, Q.; Yang, Y.; Ren, Q.; Bao, Z. Interlayer Symmetry Control in Flexible-Robust Layered Metal–Organic Frameworks for Highly Efficient C_2H_2/CO_2 Separation. *J. Am. Chem. Soc.* **2023**, *145* (36), 19903−19911. DOI: 10.1021/jacs.3c06138.

(10) Peng, Y. L.; Pham, T.; Li, P.; Wang, T.; Chen, Y.; Chen, K. J.; Forrest, K. A.; Space, B.; Cheng, P.; Zaworotko, M. J.; Zhang, Z. Robust Ultramicroporous Metal–Organic Frameworks with Benchmark Affinity for Acetylene. *Angew. Chem. Int. Ed.* **2018**, *57* (34), 10971−10975. DOI: 10.1002/anie.201806732.

(11) Li, Y. P.; Wang, Y.; Xue, Y. Y.; Li, H. P.; Zhai, Q. G.; Li, S. N.; Jiang, Y. C.; Hu, M. C.; Bu, X. Ultramicroporous Building Units as a Path to Bi-microporous Metal–Organic Frameworks with High Acetylene Storage and Separation Performance. *Angew. Chem. Int. Ed.* **2019**, *58* (38), 13590−13595. DOI: 10.1002/anie.201908378.

(12) Chen, K.-J.; Scott, H. S.; Madden, D. G.; Pham, T.; Kumar, A.; Bajpai, A.; Lusi, M.; Forrest, K. A.; Space, B.; Perry, John J.; Zaworotko, M. J. Benchmark C_2H_2/CO_2 and CO_2/C_2H_2 Separation by Two Closely Related Hybrid Ultramicroporous Materials. *Chem* **2016**, *1* (5), 753−765. DOI: 10.1016/j.chempr.2016.10.009.

(13) Lin, R.-B.; Li, L.; Wu, H.; Arman, H.; Li, B.; Lin, R.-G.; Zhou, W.; Chen, B. Optimized

Separation of Acetylene from Carbon Dioxide and Ethylene in a Microporous Material. *J. Am. Chem. Soc.* **2017**, *139* (23), 8022−8028. DOI: 10.1021/jacs.7b03850.
(14) Luo, F.; Yan, C.; Dang, L.; Krishna, R.; Zhou, W.; Wu, H.; Dong, X.; Han, Y.; Hu, T.-L.; O'Keeffe, M.; Wang, L.; Luo, M.; Lin, R.-B.; Chen, B. UTSA-74: A MOF-74 Isomer with Two Accessible Binding Sites per Metal Center for Highly Selective Gas Separation. *J. Am. Chem. Soc.* **2016**, *138* (17), 5678−5684. DOI: 10.1021/jacs.6b02030.
(15) Pei, J.; Shao, K.; Wang, J. X.; Wen, H. M.; Yang, Y.; Cui, Y.; Krishna, R.; Li, B.; Qian, G. A Chemically Stable Hofmann-Type Metal−Organic Framework with Sandwich-Like Binding Sites for Benchmark Acetylene Capture. *Adv. Mater.* **2020**, *32* (24), 1908275. DOI: 10.1002/adma.201908275.
(16) Zhang, L.; Xiao, T.; Zeng, X.; You, J.; He, Z.; Chen, C.-X.; Wang, Q.; Nafady, A.; Al-Enizi, A. M.; Ma, S. Isoreticular Contraction of Cage-like Metal–Organic Frameworks with Optimized Pore Space for Enhanced C_2H_2/CO_2 and C_2H_2/C_2H_4 Separations. *J. Am. Chem. Soc.* **2024**, *146* (11), 7341−7351. DOI: 10.1021/jacs.3c12032.
(17) Liu, R.; Liu, Q.-Y.; Krishna, R.; Wang, W.; He, C.-T.; Wang, Y.-L. Water-Stable Europium 1,3,6,8-Tetrakis(4-carboxylphenyl)pyrene Framework for Efficient C_2H_2/CO_2 Separation. *Inorg. Chem.* **2019**, *58* (8), 5089−5095. DOI: 10.1021/acs.inorgchem.9b00169.
(18) Xiang, S.-C.; Zhang, Z.; Zhao, C.-G.; Hong, K.; Zhao, X.; Ding, D.-R.; Xie, M.-H.; Wu, C.-D.; Das, M. C.; Gill, R.; Thomas, K. M.; Chen, B. Rationally Tuned Micropores within Enantiopure Metal-Organic Frameworks for Highly Selective Separation of Acetylene and Ethylene. *Nat. Commun.* **2011**, *2*, 204. DOI: 10.1038/ncomms1206.
(19) Li, Y.-Z.; Wang, G.-D.; Ma, L.-N.; Hou, L.; Wang, Y.-Y.; Zhu, Z. Multiple Functions of Gas Separation and Vapor Adsorption in a New MOF with Open Tubular Channels. *ACS Appl. Mater. Interfaces* **2021**, *13* (3), 4102–4109. DOI: 10.1021/acsami.0c21554.
(20) Li, H.-P.; Dou, Z.-D.; Wang, Y.; Xue, Y. Y.; Li, Y. P.; Hu, M.-C.; Li, S.-N.; Jiang, Y.-C.; Zhai, Q.-G. Tuning the Pore Surface of an Ultramicroporous Framework for Enhanced Methane and Acetylene Purification Performance. *Inorg. Chem.* **2020**, *59* (22), 16725–16736. DOI: 10.1021/acs.inorgchem.0c02713.
(21) Wang, L.; Sun, W.; Zhang, Y.; Xu, N.; Krishna, R.; Hu, J.; Jiang, Y.; He, Y.; Xing, H. Interpenetration Symmetry Control Within Ultramicroporous Robust Boron Cluster Hybrid MOFs for Benchmark Purification of Acetylene from Carbon Dioxide. *Angew. Chem. Int. Ed.* **2021**, *60* (42), 22865−22870. DOI: 10.1002/anie.202107963.
(22) Zhang, L.; Jiang, K.; Yang, L.; Li, L.; Hu, E.; Yang, L.; Shao, K.; Xing, H.; Cui, Y.; Yang, Y.; Li, B.; Chen, B.; Qian, G. Benchmark C_2H_2/CO_2 Separation in an Ultra-Microporous Metal–Organic Framework via Copper(I)-Alkynyl Chemistry. *Angew. Chem. Int. Ed.* **2021**, *60* (29), 15995−16002. DOI: 10.1002/anie.202102810.
(23) Liu, X.; Zhang, P.; Xiong, H.; Zhang, Y.; Wu, K.; Liu, J.; Krishna, R.; Chen, J.; Chen, S.; Zeng, Z.; Deng, S.; Wang, J. Engineering Pore Environments of Sulfate-Pillared Metal-Organic Framework for Efficient C_2H_2/CO_2 Separation with Record Selectivity. *Adv. Mater.* **2023**, *35* (20), 2210415. DOI: 10.1002/adma.202210415.
(24) Lan, H.-L.; Zheng, S.-T.; Xu, L.; Guan, G.-W.; Yang, Q.-Y. Scalable copper-based coordination frameworks with tailored pore chemistry for energy-efficient C_2H_2/CO_2 separation. *Ind. Chem. Mater.* **2025**, *3* (6), 723−731. DOI: 10.1039/d5im00068h.